Article

# Monolayer Control of Discotic Liquid Crystal by Electromigration of Dewetted Layers in Thin Film Devices

Annalisa Calo#, Pablo Stoliar, Massimiliano Cavallini, Sergey Sergeyev, Yves H. Geerts, and Fabio Biscarini

*J. Am. Chem. Soc.*, **2008**, 130 (36), 11953-11958 • DOI: 10.1021/ja801337v • Publication Date (Web): 16 August 2008



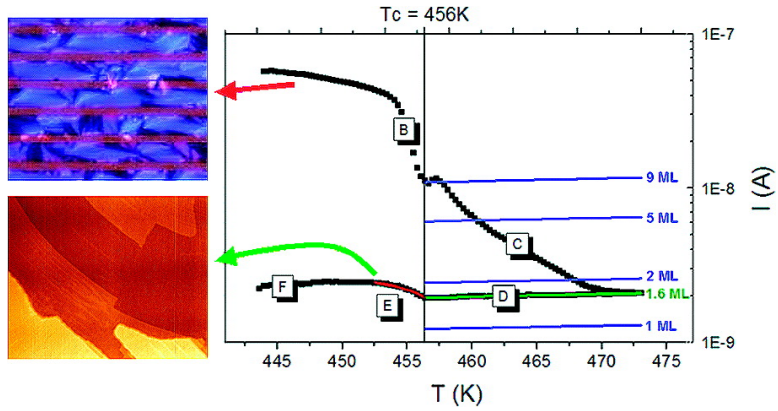


## More About This Article

Additional resources and features associated with this article are available within the HTML version:

- Supporting Information
- Access to high resolution figures
- Links to articles and content related to this article
- Copyright permission to reproduce figures and/or text from this article

View the Full Text HTML

J|A|C|S
ARTICLES

Published on Web 08/16/2008

# Monolayer Control of Discotic Liquid Crystal by Electromigration of Dewetted Layers in Thin Film Devices

Annalisa Calò,[†] Pablo Stoliar,[†] Massimiliano Cavallini,[†] Sergey Sergeyev,[‡] Yves H. Geerts,[‡] and Fabio Biscarini*,[†]

*CNR−Institute for the Study of Nanostructured Materials, Via Gobetti 101, 40129 Bologna, Italy, and Laboratory of Polymer Chemistry CP 206/1, Université Libre de Bruxelles, Boulevard du Triomphe, 1050 Bruxelles, Belgium*

Received February 22, 2008; E-mail: f.biscarini@bo.ismn.cnr.it

***Abstract:*** We show that ultrathin films of a semiconductive discotic liquid crystal, viz. phthalocyanines, can be organized to form a conductive channel tens of microns long between Au electrodes with thickness control over a single monolayer. Our approach exploits the electromigration of the isotropic phase formed starting from the pretransitional region of the columnar−isotropic phase transition. Dewetted isotropic material accumulates to the negative electrode by applying a longitudinal electric field of about 1 V/$\mu$m. Dewetting and electromigration expose an ultrathin film, a few monolayers thick, exhibiting columnar liquid crystal order. The layers of this ultrathin film melt progressively above $T_C$ and can be individually exfoliated by electromigration, starting from the ninth down to the first monolayer. The analysis of the current flowing through the junction as a function of the temperature, together with the comparative imaging of the evolution of morphology, yields a detailed picture of the changes in the dimensionality of the conductive phthalocyanine film and allows us to extract the behavior of the order parameter. The phenomenon of electromigration opens interesting questions on the technological control of individual monolayers on device patterns.

## Introduction

Liquid crystals (LC) are central materials in the technology of flat panel displays, and they are investigated as functional materials for optics and organic electronics. Disk-like (discotic) molecules, typically comprising a flat aromatic core and flexible peripheral substituents, generally exhibit columnar liquid crystalline phases and they are termed discotic liquid crystals (DLC). In DLC, the diffusion length of charge and/or excitation can be increased to several tens of nanometers, making them attractive as active materials for optoelectronic devices.[1] This implies that the molecular order and the alignment of the columns in the device channel can be governed. Field effect transistors with DLC have been demonstrated by various methods.[2–6] However, all of them either use top-contacts, aligned primer layers, or thick DLC films, whereas bottom-contact geometry represents a problem for the technology of these materials. Here we introduce a new approach, based on the electromigration of DLC in the isotropic phase across a bottom-contact device channel, to yield active transport layers made of a few monolayers of highly oriented DLC columns. We demonstrate that, owing to graded thermodynamic and rheological properties across the DLC film thickness, we can first remove an upper, more disordered, part of the film, and then cleave the residual film layer-by-layer down to a single monolayer of highly oriented columns connecting the electrodes. These results open new perspectives for the fabrication of devices based on DLC semiconductors, such as ultrathin film field effect transistors integrated in flexible active matrix displays and temperature-sensitive smart displays and windows.

## Results

In this work we use a metal-free mesogenic phthalocyanine ($H_2Pc(OC14,10)_4$, abbreviated *Pc*), shown in Figure 1e and prepared as described earlier.[7] According to the previously published data (obtained from the onsets of differential scanning calorimetry (DSC) curves), *Pc* exhibits a transition between liquid crystalline columnar rectangular ($Col_r$) and columnar hexagonal ($Col_h$) phases at 333 K, and $Col_h$ to isotropic (I) phase transition at 453 K.[7–9]

Thin films of *Pc* are spin coated on bottom-contact silicon test patterns (Figure 1a,b), yielding randomly oriented needles

[†] CNR−Institute for the Study of Nanostructured Materials.
[‡] Université Libre de Bruxelles.

(1) Sergeyev, S.; Pisula, W.; Geerts, Y. H. *Chem. Soc. Rev.* **2007**, *36*, 1902–1929.
(2) Van de Craats, A. M.; Stutzmann, N.; Bunk, O.; Nielsen, M. M.; Watson, M.; Müllen, K.; Chanzy, H. D.; Sirringhaus, H.; Friend, R. H. *Adv. Mater.* **2003**, *15*, 495–499.
(3) Pisula, W.; Menon, A.; Stepputat, M.; Lieberwirth, I.; Kolb, U.; Tracz, A.; Sirringhaus, H.; Pakula, T.; Müllen, K. *Adv. Mater.* **2005**, *17*, 684–689.
(4) Breiby, D. W.; Bunk, O.; Pisula, W.; Solling, T. I.; Tracz, A.; Pakula, T.; Müllen, K.; Nielsen, M. M. *J. Am. Chem. Soc.* **2005**, *127*, 11288–11293.
(5) Donley, C. L.; Zangmeister, A. P.; Wei, X.; Minch, B.; Drager, A.; Cherian, S. K.; LaRussa, L.; Kippelen, B.; Domercq, B.; Mathine, D. L.; O'Brien, D. F.; Armstrong, N. R. *J. Mater. Res.* **2004**, *19*, 2087–2099.
(6) Charlet, E.; Grelet, E.; Brettes, P.; Bock, H.; Saadaoui, H.; Cisse, L.; Destruel, P.; Gherardi, N.; Seguy, I. *Appl. Phys. Lett.* **2008**, *92*, 024107.
(7) Tant, J.; Geerts, Y. H.; Lehmann, M.; De Cupere, V.; Zucchi, G.; Laursen, B. W.; Bjornholm, T.; Lemaur, V.; Marcq, V.; Burquel, A.; Hennebicq, E.; Gardebien, F.; Viville, P.; Beljonne, D.; Lazzaroni, R.; Cornil, J. *J. Phys. Chem. B* **2006**, *110*, 3449–3449.
(8) De Cupere, V.; Tant, J.; Viville, P.; Lazzaroni, R.; Osikowicz, W.; Salaneck, W. R.; Geerts, Y. H. *Langmuir* **2006**, *22*, 7798–7806.

  

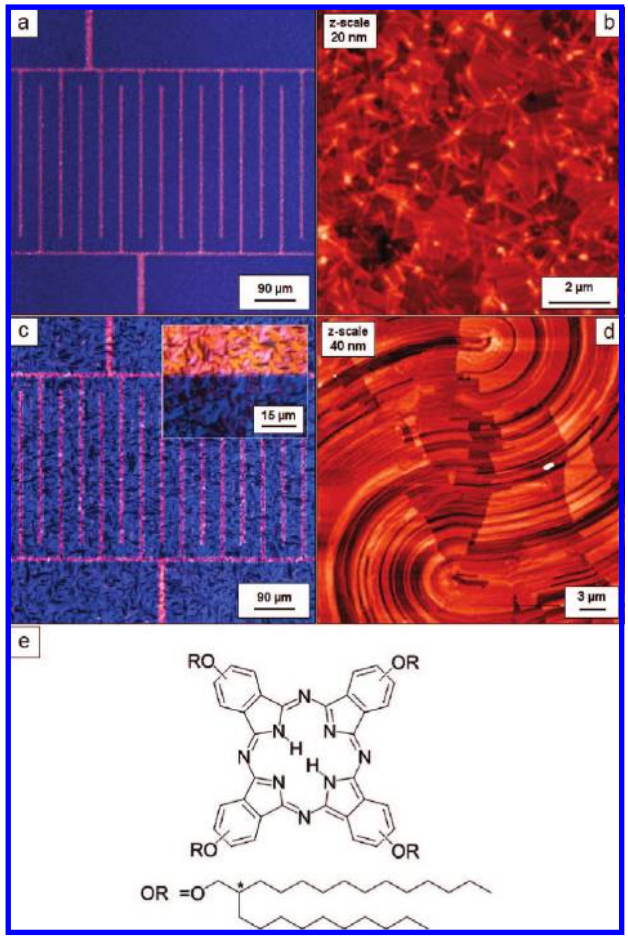


***Figure 1.*** Morphology of DLC films on a test pattern device. (a,b): spin coated film ($h$ = 150 nm) before the thermal treatment; (c,d): bulk material after the thermal treatment. Images (a,c) have been acquired with POM; (b,d) corresponding AFM images. (e) Chemical structure of $H_2Pc(OC14,10)_4$.

whose characteristic size is 0.5 $\mu$m (Figure 1b). These features have been extensively discussed in ref 8. We then performed a thermal cycle heating the film at the melting point and then cooling to RT in order to increase the molecular order. In the optical image (Figure 1c), large fan-shaped domains, which exhibit homogeneous colors and a characteristic size, can be easily observed. Figure 1d is the high magnification AFM image on a region of Figure 1c. The DLC columns are not resolved, but they are oriented normal to the lamellae.[8] Uniaxial alignment of the columns is achieved across a few micrometer lateral length scale and it breaks down owing to the curvature of the lamellae. Upon our experimental conditions the ordered columns of *Pc* molecules lie parallel to the substrate (edge-on alignment).[8] This is confirmed by polarized light optical microscopy with cross polarizers (POM) (Figure 1C) and by high resolution AFM imaging (see Figure 4 below). In no case did we succeed in healing the domain boundaries, yielding complete uniaxial alignment.[10]

Although we observed by POM the beginning of the transition from the $Col_h$ to the I phase at 453 K, the birefringence of the films completely disappears only at 456 K. Hence, here we prefer to define $T_C$ = 456 K as the temperature for the phase transition $Col_h$−I, in a sense that above this temperature only the isotropic phase is observed. The temperature range 453−456 K is called here the "pre-transitional region".

Starting from the pretransitional region the DLC films become unstable and dewet, leaving a pattern of droplets homogeneously distributed on the surface. This happens also in the absence of electric field. When an electric field across the channel is turned on we observe the migration of the largest fraction of the dewetted DLC layers from one electrode to the other (Figure 2b−d and f−h), resulting in the accumulation of large sessile drops of DLC at the negatively charged electrode in a second time scale (see below). If we switch off the electric field after the complete accumulation of the material on the negative electrode, we observe the immediate relaxation of the material and, in a longer time scale (minutes) the spreading of the DLC on the surface until a contact angle is achieved (typically 7° at RT). This quick relaxation resembles phenomenologically the electrowetting effect described in literature.[11,12]

If the temperature decreases without turning off the electric field, the isotropic droplets undergo the transition to the $Col_h$ phase, giving rise to large domains exhibiting the characteristic birefringence (Figure 2e and i). We never observe, even after many days, a modification of the shape of these domains. The action of the electric field is to displace and remove the dewetted material by electromigration.[13] In the following we analyze the electromigration phenomenon depicted in Figure 2 as a function of the electric field at different temperatures.[14,15]

Figure 3 shows the velocity of migration $v_E$ vs the electric field. The migration requires a threshold field above 0.40 ± 0.25 V/$\mu$m. Above this, $v_E$ increases linearly for fields ranging from 0.25 to 2 V/$\mu$m. The inset shows the trend of $v_E$ vs temperature for different electric fields; the minimum temperature $T_{min}$ at which the phenomenon occurs is estimated to be 452 ± 2 K by extrapolation of the data to $v_E$ = 0. This temperature of about 453 K coincides with the temperature at which the film undergoes dewetting[16–19] (notice the extensive film rupture into droplets[20,21] in the regions outside the electrodes in Figure 2).

In spite of the fact that a substantial fraction of the bulk material migrates upon the application of the electric field, a continuous layer remains steadily anchored to the substrate between the contacts.[22–24] This is apparent from the evolution of the morphology shown as a sequence of AFM images in

(9) Gearba, R. I.; Bondar, A. I.; Goderis, B.; Bras, W.; Ivanov, D. A. *Chem. Mater.* **2005**, *17*, 2825–2832.
(10) Mouthuy, P. O.; Melinte, S.; Geerts, Y. H.; Jonas, M. *Nano Lett.* **2007**, *7*, 2627–2632.
(11) Mugele, F.; Baret, J.-C. *J. Phys.: Condens. Matter* **2005**, *17*, R705–R774.
(12) Voicu, N. E.; Harkema, S.; Steiner, U. *Adv. Funct. Mater.* **2006**, *16*, 926–934.
(13) Lin, Z.; Kerle, T.; Russell, T. P.; Schäffer, E.; Steiner, U. *Macromolecules* **2002**, *35*, 6255–6262.
(14) Imura, H.; Okano, K. *Jpn. J. Appl. Phys* **1972**, *11*, 1440–1445.
(15) Mundy, C. J.; Levin, Y.; Dawson, K. A. *J. Chem. Phys.* **1992**, *97*, 7695–7698.
(16) Reiter, G. *Phys. Rev. Lett.* **1992**, *68*, 75–78.
(17) Reiter, G.; Khanna, R. *Langmuir* **2000**, *16*, 6351–6357.
(18) Brochard-Wyart, F.; de Gennes, P. G.; Hervert, H.; Redon, C. *Langmuir* **1994**, *10*, 1566–1572.
(19) Wyart, F. B.; Martin, P.; Redon, C. *Langmuir* **1993**, *9*, 3682–3690.
(20) Seemann, R.; Herminghaus, S.; Jacobs, K. *J. Phys.: Condens. Matter* **2001**, *13*, 4925–4938.
(21) Seemann, R.; Herminghaus, S.; Jacobs, K. *Phys. Rev. Lett.* **2001**, *86*, 5534–5537.
(22) Barbero, G.; Durand, G. *J. Appl. Phys.* **1991**, *69*, 6968–6973.
(23) van Effenterre, D.; Ober, R.; Valignat, M. P.; Cazabat, A. M. *Phys. Rev. Lett.* **2001**, *87*, 125701(1−4).
(24) van Effenterre, D.; Valignat, M. P.; Roux, D. *Europhys. Lett.* **2003**, *62*, 526–532.

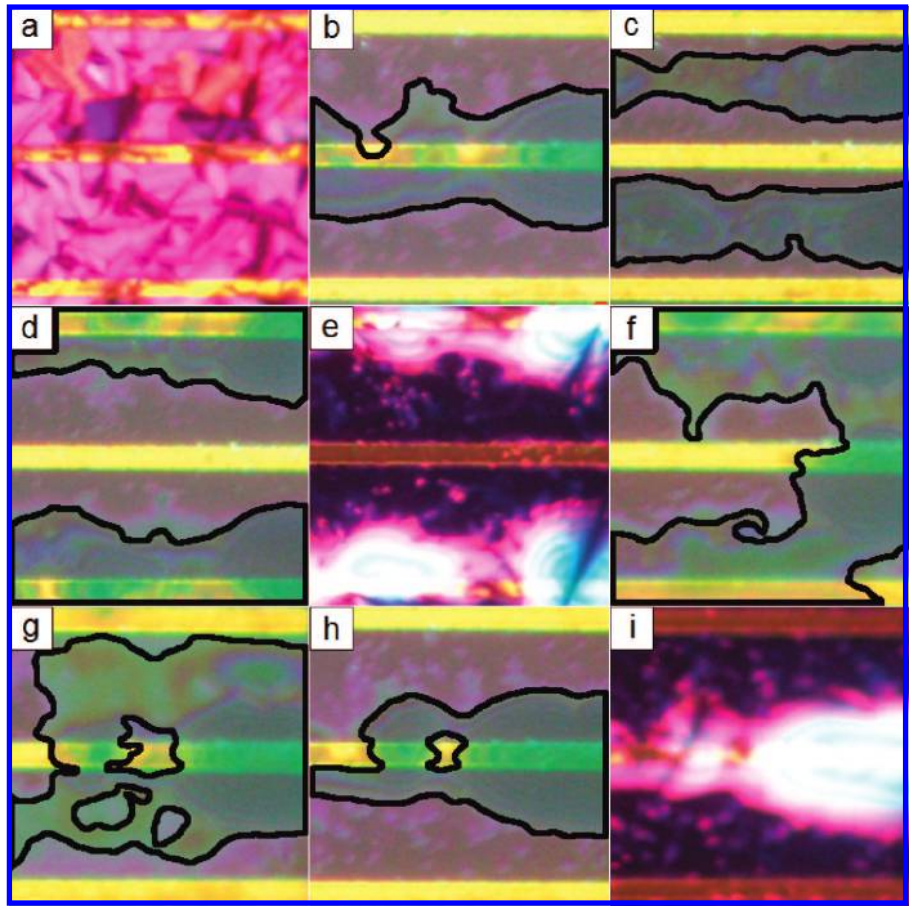


***Figure 2.*** Dynamics of DLC film under electric field observed by POM (we indicate with black contours the regions where there is a large amount of DLC in the isotropic phase): the ordered spin coated film (a) is heated over the melting point $T = 460$ K (b); the material moves across the channel (c) from the positive electrode (central) to the adjacent negative finger electrodes (top and bottom); cooling to 433 K (e) results into the accumulation of large amount of anisotropic DLC drops at the negatively charged electrodes. The typical birefringent features of the $Col_h$ appear. Repeating the same process as (b−d) with reversed bias (f−i), leads to the migration of the larger amount of material to the central electrode (now negatively biased). Applied electrical field is $\pm 1$ V/$\mu$m. Images are 55 $\mu$m wide. See movie in the Supporting Information.

Figure 4a–c. It is clear that the rough film imaged at zero field becomes progressively thinner and a layered morphology appears. The histogram of Figure 4c (inset) evidences the layered structure with an average pitch between maxima equal to (2.82 $\pm$ 0.5) nm. This value matches the expected interlayer distance of 2.84 nm between packed columns with the disks oriented edge-on with respect to the substrate.[7,8] High-resolution AFM image in Figure 4d reveals closely packed aligned columns, with intercolumnar distance of 3.28 nm, as inferred from the respective 2D FFT shown in the inset. This value corresponds to the *b*-axis length (3.25 nm) of the $Col_r$ structure.[7,8] This evidence demonstrates that the interfacial layers are highly oriented and molecularly ordered, despite of the massive displacement of the bulk material upon the applied field.

The inferred reorganization process is schematically depicted in Figure 4e−h. Dewetting of the continuous film into microscopic droplets occurs in the pretransitional region, and their displacement is driven by the electric field. Whereas the bulk material is displaced, the interfacial layers with the substrate are immobilized. Molecular order in these layers increases in the proximity of the substrate as observed by comparing the AFM images of Figure 4c and d with Figure 4a. This behavior is explained as the interaction with the substrate stabilizes the mesophase, shifting the onset of the $Col_h$−I transition at higher temperatures.[25–27]

The stabilization of a molecularly ordered film, with a thickness corresponding to only a few monolayers has important consequences on the charge transport behavior. In Figure 5 (top), we show the electrical current flowing across the channel as a function of temperature at a constant electric field of 1 V/$\mu$m. This voltage biases the device for the electrical transport measurement and generates the electric field necessary for the electromigration. The data correspond to a heating−cooling cycle in the range 343−473 K. First, we notice that currents of 1−10 nA are driven through the junction, indicating that *Pc* is already doped. Thus, the system is governed by conductivity rather than field effect mobility.[28] We identify different regions in conjunction with the optical microscopy observation: a region A (343−453 K), where there are no changes in the geometry of the DLC thin film; a pretransitional region B (453−456 $K = T_C$) where mass displacement is observed; a region C above $T_C$

(25) Moldovan, R.; Tintaru, M.; Beica, T.; Frunza, S. *Cryst. Res. Technol.* **1999**, *34*, 1315–1321.
(26) Evangelista, R. L.; Barbero, G. *Phys. Rev. E* **1993**, *48*, 1163–1171.
(27) Barbero, G.; Evangelista, L. R.; Giocondo, M.; Ponti, S. *J. Phys. II* **1994**, *4*, 1519–1540.
(28) Brown, A. R.; Jarrett, C. P.; de Leeuw, D. M.; Matters, M. *Synth. Met.* **1997**, *88*, 37–55.

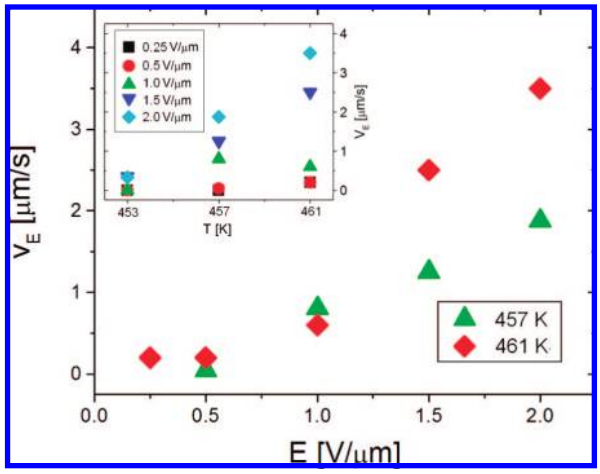


***Figure 3.*** Velocity of migration versus electrical field for $T = 457$ and 461 K. (Inset) Trend of $v_E$ vs $T$ for the different electric fields.

where drops of displaced material appear isotropic but the ordered ultrathin layer is present; a region D where drops are still isotropic and the ultrathin layer does not exhibit optical contrast; a region E where drops give rise to birefringence; region F where their transition to $Col_h$ mesophase is completed.

In this region, the current first increases up to about 380 K, then it flattens out and decreases. The rising part is fit to an Arrhenius type behavior, with activation energy of $(0.243 \pm 0.06)$ eV, which is consistent with reported activation energies of analogous molecules.[29,30] In region A the temperature effect on charge transport wins over the increasing disorder of the mesophase up to 380 K, then the latter dominates. This trend reminds earlier microwave charge transport measurements.[31,32]

In region B at $T > 453$ K a sudden drop in the current is observed as the fluidity starts to increase and the electrical field displaces the bulk material across the channel. This regime is dominated by the variation in the cross-section of the channel, viz. the effective decrease of thickness $h$. This is even more apparent in Figure 5 (bottom), whose data are acquired across the $Col_h-I$ transition. Just above $T_C = 456$ K (region C) the current exhibits an inflection point or a plateau, then it decreases. The nonmonotonic behavior can be ascribed to the stabilization of the film thickness (i.e., the bulk part has completely migrated away) and a subsequent alignment of the columns between the electrodes. From the AFM images we infer that the corresponding thickness is 9 ML. The ratio between the apparent current plateau before the pretransitional region and the current above the $Col_h-I$ transition is about five, suggesting that the scaling of the current closely follows the decrease in thickness of the active layer.

At temperatures higher than $T_C$ the current decreases exponentially with the temperature with a decay rate equal to 0.135 $K^{-1}$. This corresponds to a progressive removal of stable monolayers with an effective rate ranging from about 2 to 0.4 ML/K. Thus, we control the effective thickness of the interfacial layer with an accuracy of a single layer, upon controlling the T with an accuracy better than 1 K. The current values corresponding to 1, 2, 5, and 9 ML are indicated. At 473 K, the film thickness is $1 \pm 0.5$ ML, thus the device operates only with 1−2 ML thick film. Thickness control is particularly relevant in view of FET applications, where the active layer consists only of the very few ML in contact with the gate dielectric.[33]

The fact that the current does not decrease stepwise can be ascribed to the distribution of internal energy in the finite assembly of columns. This is broadly due to finite size effects and the presence of different intermolecular interactions within and between columns, and depends on the nonideal stacked morphology (as in Figure 4 c). These factors contribute to smooth out the possible discrete steps from the dewetting of each monolayer.

The result of electromigration is irreversible. Cooling down from 473 K does not allow the film to recover the displaced monolayers. In region D (473−456 K) the current decreases monotonically (it appears as a plateau in log scale). This portion can be fit to an Arrhenius law with $I_{0D} = (11.0 \pm 0.7)$ nA and $E_{0D} = (0.068 \pm 0.003)$ eV. This indicates that neither the geometrical parameters nor the order parameter is changing, and the temperature is affecting only the hopping rate. Interestingly the activation energy in this region, where the film consists of highly ordered uniaxially oriented columns, is about three times smaller than the activation energy measured in region A. This may reflect the scaling of dimensionality from 3D in region A to 1D in region D.

In region E, as the DLC droplets on the electrodes start to exhibit birefringence, due to the formation of columnar domains at $T_C = 456$ K (see also Figure 2), an increase in current is observed. We ascribe this effect to an improved contact between the first monolayer and the electrodes. This may be due either to the formation of ordered domains across, which facilitate charge injection, or else to a wider cross-section at the contacts.

## Discussion

We account for the observed behavior of the current vs $T$ using a simple phenomenological expression:

$$I(T) = E \cdot W \cdot h(T,E) \cdot S(T,E) \cdot \sigma_{CRYST} \cdot \exp\left(-\frac{T_0}{T}\right) = I_0 \cdot S(T,E) \cdot \exp\left(-\frac{T_0}{T}\right) \quad (1)$$

where $E = V/L$ is the electric field, $V$ is the applied voltage, $W$, $h$, $L$ are the channel width, height, and length respectively; $\sigma_{CRYST}$ is the conductivity of a perfectly ordered $Pc$ crystal. Here we ignore the presence of other mesophases, since we are considering only the experimental data across the $Col_h-I$ transition.

The conductivity of the ordered system is modulated by an order parameter dependent term $S(T, E)$ which is sensitive to the orientational order (in terms of alignment of the columns and intra-columnar orientation of the molecules along the stack), the correlation length scale along the columns and the packing density of the columns. The exponential term represents the hopping contribution with activation barrier $T_0$.

(29) Ray, A. K.; Nabok, A.; Hassan, A. K.; Cook, M. J. *IEEE Proc. - Circuits Devices Syst.* **1999**, *146*, 44–48.
(30) Wright, J. D. *Prog. Surf. Sci.* **1989**, *31*, 1–60.
(31) Schouten, P. G.; Warman, J. M.; De Haas, M. P.; van Nostrum, C. F.; Gelinck, G. H.; Nolte, R. J. M.; Copyn, M. J.; Zwikker, J. W.; Engel, M. K.; Hanack, M.; Chang, Y. H.; Ford, W. T. *J. Am. Chem. Soc.* **1994**, *116*, 6880–6894.
(32) Debije, M. G.; Jorge Piris, J.; de Haas, M. P.; Warman, J. M.; Tomovic, Z.; Simpson, C. D.; Watson, M. D.; Mullen, K. *J. Am. Chem. Soc.* **2004**, *126*, 4641–4645.
(33) Dinelli, F.; Murgia, M.; Levy, P.; Cavallini, M.; Biscarini, F.; de Leeuw, D. M. *Phys. Rev. Lett.* **2004**, *92*, 116802.

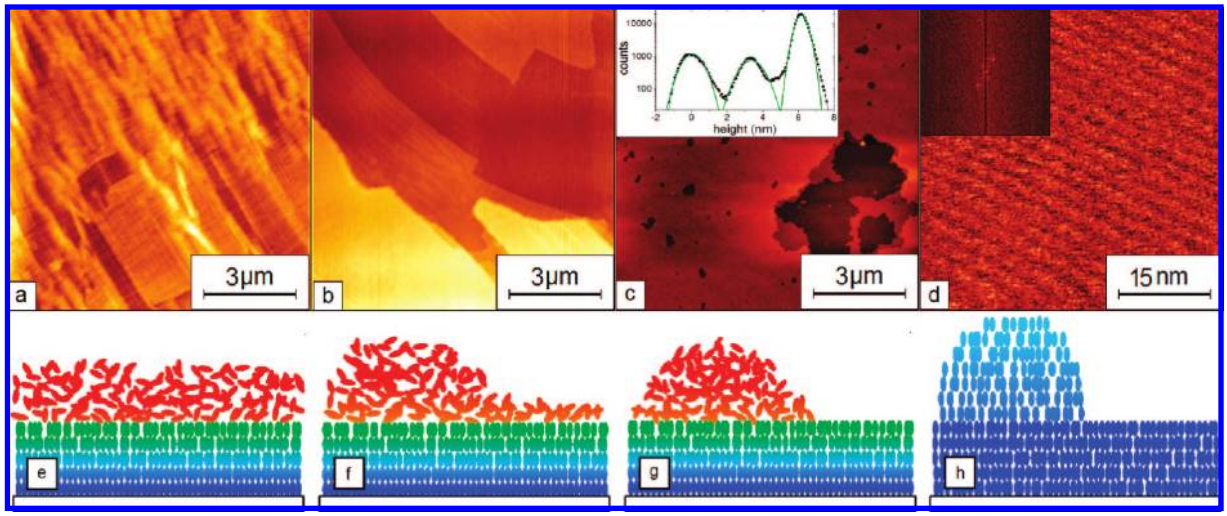


***Figure 4.*** AFM images of *Pc* film (a) before the electromigration process displaces the bulk material on top. Films (b) 9 ML and (c) 2 ML thick, remaining in the channel of the device after the film has been heated at 456 and 473 K respectively with the electric field applied. (Inset of c) Height distribution histogram for the 2 ML film. (d) High resolution AFM image of the film in (c) showing ordered columns of *Pc* molecules with a periodicity of 3.28 nm as extracted from the 2D FFT (inset). AFM images are acquired at RT. (e−g) Schematic drawing of the migration of *Pc* molecules at *T* about 460 K. (h): dewetted film at room temperature. The color scale in the schematic drawing represents the fluidity of molecules, viz. blue: low, red: high.

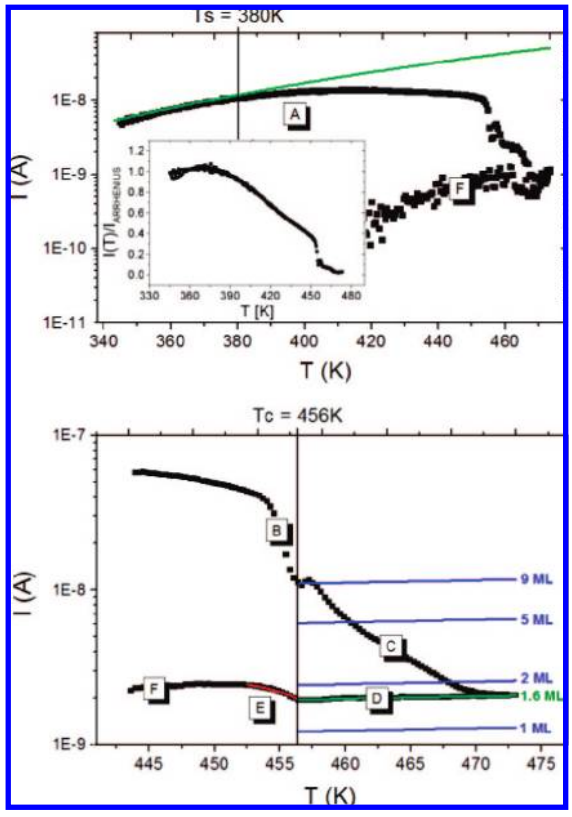


***Figure 5.*** Electrical current at 20 V vs temperature. (Top) Response of annealed DLC film at *T* between 343 and 473 K; the green straight line represents the Arrhenius fit with 0.243 eV activation energy. (Inset) Ratio between this ideal Arrhenius conduction and the measured value. (Bottom) Detail of the current at *T* between 443 and 473 K. The red curve corresponds to a conduction model as the one reported in eq 1 with $S(T) \propto ((T_C - T)/T_C)^{\beta}$. For $T_C = 456$ K best fit yields $\beta = (0.74 \pm 0.04)$. The green line indicates the Arrhenius fit for the 1.6 ML film, with activation energy of 0.068 eV. Horizontal blue lines are scaled for different thicknesses of the steadily anchored layer.

In this framework, without detailing a precise functional dependence of $S(T, E)$, we infer that:

(i) region A is dominated by the hopping rate for $T <$ 380 K.

(ii) region B arises from the variation of $S(T, E)$ and also $h(T, E)$ by electromigration, the latter occurring in the range 453 K $< T <$ 456 K; the latter features depend on the heating rate and it is a kinetic effect. Thickness $h$ varies from 150 to 27 nm in a temperature interval of 3 K, while $S$ decreases as a power law. If we assume that the power law is similar to the one measured in region E of Figure 5 (see also below), then we infer that, in the pretransitional region, electromigration and the subsequent variation of $h$ represent the main contributions to the changes in the current (see Supporting Information).

(iii) region C is dominated by the reduction of $h(T, E)$ layer-by-layer for temperatures above $T_C$; here the bulk order parameter is zero, whereas the order parameter of the interfacial layers decreases smoothly.[34] The transition to isotropic phase in the upper layers takes a second order character. The number of stable monolayers is the outcome of the tradeoff between the bulk elastic free energy and the surface potential energy. In fact, the layers of discotic molecules near the substrate experience an elastic force connecting the surface molecules to the bulk[27–35] and a substrate aligning force. For example, in the situation depicted in Figure 4g the number of stable monolayers is 5 according to the results in Figure 5 (bottom) for $T = 460$ K. The material in proximity of the substrate remains with a higher $S$ and it has no enough fluidity to be displaced by the electric field.

(iv) region D is dominated by hopping in a quasi-monolayer DLC film; order parameter is constant or slightly increasing.

(v) region E is dominated by the increase of $S(T, E)$ in the pretransitional region.

(vi) region F is governed by hopping at lower temperatures with an activation energy (0.195 eV) similar to region A.

By dividing the data in Figure 5 (top) (and represented by eq 1) by the hopping term $I_{0A} \cdot \exp(-T_{0A}/T)$ from region A, we extract the behavior of the effective order-parameter dependent $S(T, E)$. The result is shown in the inset of Figure 5 (top). It

(34) Sheng, P. *Phys. Rev. Lett.* **1976**, *37*, 1059–1062.
(35) Moldovan, R.; Mezincescu, N. *Rom. J. Phys.* **2006**, *51*, 401–409.

clearly shows the progressive decrease of order in the pretransitional region.

A final consideration concerns the origin of the electromigration toward the negative electrodes.

*Pc* comprises a statistical mixture of four different structural isomers.[7] None of these isomers possesses a strong permanent dipole. In our geometry a dipole would be oriented and move to the closer electrodes producing an equal accumulation of material on both the electrodes. For this reason electromigration can only arise from charged species. The *Pc* batch used in this study does not contain a significant amount of inorganic impurities (see Supporting Information of ref 7), and they are not sufficient to explain such a displacement, which involves all the material in the liquid phase. The occurrence of an asymmetric electromigration to the negative electrode can be explained by an oxidation of *Pc* at the positively charged electrode (anode) followed by the migration of the injected holes on the other electrode (cathode). Indeed, the holes injection at the anode is possible because of the similarity between Au Fermi level (5.2 eV) and the HOMO of *Pc*. As reported in the Supporting Information of ref 7, the energies of *Pc* HOMO and LUMO are 5.42 and 1.54 eV, respectively. A second possible explanation concerns the possibility that the electrostatic longitudinal field induces a gradual change in the surface tension at the top of the anchored layer. This would create a gradient for the diffusion of the dewetted drops. However both of these hypotheses require further detailed investigations, including a characterization of the charged species present or generated in DLC and comparison with simulations of discotic liquid crystals.

## Conclusions

In conclusion we demonstrated a viable method to yield highly oriented films of DLC, having a few monolayer thickness and bridging the channel of a device with tens of $\mu$m channel length. This is achieved by controlling the entangled phenomena of dewetting and electromigration in DLC films on a device structure, as temperature is swept across $Col_h$ phase into the isotropic phase and electric field is applied across the channel of the device. The structural and morphological changes experienced by the active DLC layer can be transduced into the electrical current, the latter used to monitor the order parameter of the DLC. This approach represents a powerful tool for aligning DLC in a bottom-electrode device channel. It may also be exploited, more generally, for stabilizing and optimizing the device performance of other classes of mesogenic organic semiconductors in ultrathin film devices.

## Experimental Methods

**Films Preparation.** The films were prepared by spin coating *Pc* solutions in heptane; the films height depends mainly on the *Pc* concentration and on the angular velocity of the spin coater. We characterize the film thickness with respect to the angular speed (from 1500 to 6000 rpm) and the *Pc* concentration (20 − 6.3 − 2 − 0.05 mg/mL) by AFM measurements. We found an excellent agreement with $h = 4423 \cdot \omega^{-0.77} \cdot C^{0.76}$, where $h$ is the film thickness in nm, $\omega$ the angular speed in rpm, and $C$ the concentration in mg/mL.[36]

A key point in the film fabrication is the "chemical" contamination of *Pc*, presumably due to solvent residuals remained from the spin coating process and/or to atmospheric contamination.[37] Even if we did not perform a detailed analysis, we usually observed a shift (going down until 433 K) and a broadening of the $Col_h$−I transition in the DLC films. We completely suppressed this problem backing the films in vacuum (0.01 mbar) at 40 °C for 15 min before performing the annealing procedure. All the experiments reported in this work were performed keeping the films in vacuum at 0.01 mbar.

**Thermal Cycles.** All the thermal cycles where performed inserting the samples in a Linkam TMHS 600 heating stage connected to a TP-94 temperature controller. The cycle to increase the order in the films are performed going to 460 K at a rate of 90 K/min and immediately returning to 443 K with a cooling rate of 90 K/min, and then to RT without controlling the rate. The heating/cooling cycle performed at different rates gives different domain sizes but not a substantial difference in the electrical measurements was observed. Domain size changes with the cooling rate, specifically at 90 K/min the domain size is 27 $\mu$m and at 10 K/min is 70 $\mu$m, as measured from the characteristic frequency of the power spectrum density (PSD) of the AFM topography. The current measurements were acquired during a thermal cycle of heating and cooling at the rate of 1 K/min.

**AFM Measurements.** The film thickness, before and after the electromigration process, together with the film morphology were measured with a Smena AFM (NT-MDT, Moscow, Russia). The AFM images were obtained at room temperature, by tapping mode in air. Commercial Au coated silicon tips were used with a typical curvature radius of 10 nm (NSG 10/50) to collect 512 × 512 pixels images.

Thickness was measured from AFM images of regions where extended defects (like the one shown in Figure 4c) are present. This occurrence is sufficiently frequent to encounter as the film dewets. The stated thickness relies on the histogram of topography, as the one shown in the inset of Figure 4c. The phase contrast, equal for the terraces and different for the lowest features, allows us to assign with some confidence the lowest features to the substrate. When continuous films were imaged, we made a groove with a scalpel, and then measured the height across.

**Image Analysis.** The analysis of the AFM and optical images was performed using the Gwyddion 2.9 software (http://gwyddion.net/).

**Electromigration Velocity.** Velocity of the electromigration was measured from experiments as presented in Figure 2 at different temperatures (453, 457 and 461 K) and electrical fields (0.25−2 V/$\mu$m) taking images every 2 s. From these images we measured the displacement front and then determined the speed as the ratio between the channel length and the time the material travel along it.

**Electrical Measurements.** For the electrical measurements, a film of about 150 nm was deposited by spin coating on the test pattern with bottom contacts. These contacts (150 nm of Au + Cr adhesion layer on a 200 nm-thick thermal $SiO_x$ substrate) form an interdigitated 2-terminal device with a channel length of 16 mm and width 20 or 40 $\mu$m. A Keithley 2602 SourceMeter biases the channel and measures the current.

**Acknowledgment.** We thank Claudio Zannoni, Luca Muccioli, Roberto Berardi and Luis Eduardo Hueso Arroyo for useful discussions. This work is supported by projects EU-STRP 033355 STAG (A.C.), EURYI-DYMOT (M.C., P.S.).

**Supporting Information Available:** A movie showing the electromigration process and the information about the theoretical derivation of the main contributions to current in region B is available. This material is available free of charge via the Internet at http://pubs.acs.org.

JA801337V

(36) Meyerhofer, D. *J. Appl. Phys.* **1978**, *49*, 3993–3997.
(37) Bohrer, F. I.; Sharoni, A.; Colesniuc, C.; Park, J.; Schuller, I. K.; Kummel, A. C.; Trogler, W. C. *J. Am. Chem. Soc.* **2007**, *129*, 5640–5646.